Available online at www.sciencedirect.com
ScienceDirect
Journal of Photochemistry and Photobiology A: Chemistry 190 (2007) 94–100
Journal of Photochemistry and Photobiology A:Chemistry
www.elsevier.com/locate/jphotochem

Bactericidal activity of nitrogen-doped metal oxide nanocatalysts and the influence of bacterial extracellular polymeric substances (EPS)

Yang Liu [a], Jin Li [a,*], Xiaofeng Qiu [b], Clemens Burda [b,*]

[a] *Department of Civil Engineering and Mechanics, University of Wisconsin-Milwaukee, Milwaukee, WI 53201, USA*
[b] *Center of Chemical Dynamics & Nanomaterials Research, Department of Chemistry, Case Western Reserve University, Cleveland, OH 44106, USA*

Received 2 January 2007; received in revised form 23 February 2007; accepted 19 March 2007
Available online 23 March 2007

Abstract

The antibacterial effect of nitrogen-doped TiO_2 and ZrO_2 were tested on *Escherichia coli* and biofilm heterotrophic bacteria under solar light illumination. The rates of photocatalytic inactivation for biofilm bacteria with soluble extracellular polymeric substances (EPS) stripped off and *E. coli* bacteria were found to be higher than those of the biofilm bacteria with intact EPS. Measurements of both bacterial count and cellular components (carbohydrate and protein) revealed that EPS play an important role in controlling the kinetics of solar-induced photocatalysis. $TiO_{2-x}N_x$ and $ZrO_{2-x}N_x$ doped with ethylenediamine as the nitrogen source showed improved photoactivity compared with $TiO_{2-x}N_x$ using ethanolamine as the nitrogen source.

Keywords: Bacteria inactivation; Extracellular polymeric substances (EPS); Solar light; Titanium dioxide; Nitrogen-doped nanoparticles

1. Introduction

Heterogeneous photocatalysis based on the interaction of light with nanoparticles has emerged as an innovative and promising technique for water and wastewater purification [1–3]. Among various materials being developed for photocatalytic applications, titanium dioxide (TiO_2) has received great attention because of its high reactivity and chemical stability under UV light irradiation ($\lambda < 390$ nm) [1–5]. However, due to its wide band gap (~3.2 eV), TiO_2 can only be used in the UV region, which accounts for less than 5% of the solar spectrum, whereas the visible light represents about 45% of the solar energy. In recent years, interest has grown in shifting the optical response of TiO_2 from UV to the visible spectrum in order to improve the efficiency of TiO_2 photocatalysis. Selectively doping TiO_2 is believed to be one of the most effective ways to change the intrinsic band structure of TiO_2, which can promote the photocatalytic activity by enhancing the visible light sensitivity [6–10]. Among various dopants, nitrogen is regarded as the most promising doping element because of its similar properties compared with oxygen [7,8]. To date, one of the most efficient approaches to synthesize nitrogen-doped TiO_2 nanoparticles seems to be the wet chemical approach [11–15]. Recently, we developed a chemical method to incorporate nitrogen into TiO_2 and ZrO_2, which are group IVB metal oxide nanoparticles [16]. The nitrogen-doped TiO_2 nanoparticles showed enhanced visible light absorption and better photocatalytic performance on methylene blue and azo dye decomposition than pure TiO_2 [17,18].

The bactericidal effect of TiO_2 generally has been attributed to the decomposition of bacterial outer membranes by reactive oxygen species (ROS), primarily hydroxyl radicals ($^{\bullet}OH$), which leads to phospholipid peroxidation and ultimately cell death [19–25]. Gogniat et al. pointed out that the aggregation of bacteria onto TiO_2 particles is the key step in photokilling because hydroxyl radicals have an extremely short lifetime (10^{-9} s) and must be generated near the cell membrane [22]. Cho et al. [21] studied the photocatalytic inactivation behavior of MS-2 phage and *Escherichia coli* bacteria and concluded that the biocidal models of ROS act differently depending on the specific microorganism. Both the free and surface-bound hydroxyl radicals, as well as other ROS, such as $O_2^{\bullet -}$ and

* Corresponding authors. Tel.: +1 414 229 6891; fax: +1 414 229 6958.
E-mail addresses: li@uwm.edu (J. Li), burda@case.edu (C. Burda).

1010-6030/$ – see front matter © 2007 Elsevier B.V. All rights reserved.
doi:10.1016/j.jphotochem.2007.03.017

H_2O_2, were reported to be involved in the *E. coli* inactivation [21].

Planktonic bacteria were used as model organisms in most research on the bactericidal effect of TiO_2. However, more than 99% of the bacteria exist in the form of biofilms in natural environment [26]. Biofilms are also ubiquitous in engineered water and wastewater treatment systems. Although the majority of bacteria entering a drinking water facility are planktonic, biofilms may form during a number of processes, e.g., water utilities frequently use biofilters, which are of the biofilm type, to remove biodegradable organic matter (BOM) and reduce disinfection byproducts (DBP) formation [27]. Recent studies conducted in drinking water and reclaimed water distribution systems have also demonstrated the presence of biofilms and their association with pathogenic organisms [27]. In a typical biofilm, up to 90% of the organic carbon is EPS, which contains macromolecules that are produced and secreted by the cells, the cellular debris and the products of extracellular hydrolytic activity [26,28]. The presence of EPS has a significant impact on the bacterial surface characteristics and may determine the adhesion of bacteria to TiO_2 particles [28]. Moreover, the protective layer formed by EPS can cushion microorganisms against the oxidative power of ROS.

The goal of this study is to illustrate the role of EPS in the photodegradation of bacteria under solar light illumination. The performance of newly synthesized nitrogen-doped nanoparticles ($TiO_{2-x}N_x$, $ZrO_{2-x}N_x$) and pure TiO_2 was systematically evaluated in terms of their bactericidal activity on three different types of bacteria, i.e., biofilm bacteria covered with EPS, bacteria with their soluble EPS stripped off, and *E. coli* bacterial cells. The effect of semiconductor photocatalysis on the oxidation of cellular components, including total carbohydrate and total protein was examined.

2. Materials and methods

2.1. The preparation and characterization of nanoparticles

The nitrogen-doped TiO_2 and ZrO_2 nanoparticles were prepared from a precursor solution of 4 mL $Ti[OCH(CH_3)_2]_4$ (Aldrich, 97%) or $Zr[OCH(CH_3)_2]_4$ (Aldrich, 70%), ethylenediamine (Strem, 99%) or ethanolamine (Aldrich, 99%) and 200 mL of anhydrous ethanol. The precursor solution was refluxed for 24 h and hydrolyzed by adding drop-wise 20 mL distilled water. The yellow precipitates were centrifuged and dried under vacuum. The resulting powders were then sintered in the air at 200 °C for 1 h [16]. The nitrogen-doped TiO_2 and ZrO_2 nanoparticles were characterized by X-ray photoelectron spectroscopy (XPS) (Perkin-Elmer Inc., MA) and UV–vis reflectance spectroscopy (Varian Inc., CA). Pure TiO_2 nanoparticles were prepared as previously reported [23]. Briefly, 10 mL of $Ti[OCH(CH_3)_2]_4$ and isopropyl alcohol (5:95 volume ratio) was slowly added into 100 mL of distilled water at pH 2 adjusted by HNO_3. The mixture was stirred for 12 h and then centrifuged. The precipitate was washed and dried under vacuum. The particle sizes were calculated from XRD patterns by the Scherrer equation for $TiO_{2-x}N_x$ (10 nm) and for $ZrO_{2-x}N_x$ (30 nm). TEM analysis also confirmed the size of these nanoparticles [16]. BET surface area measurements on these samples resulted in 80–120 m^2/g.

2.2. Biofilm development, sampling and characterization

Aerobic heterogeneous biofilms were cultivated in a continuous flow, completely mixed laboratory-scale rotating drum biofilm reactor as described by Li and Bishop [29]. The reactor was seeded with activated sludge from an aeration basin at the Jones Island wastewater treatment plant in Milwaukee, WI, USA. Synthetic wastewater with a chemical oxygen demand (COD) of 150 mg/L was continuously pumped into the reactor with a hydraulic retention time of 2 h. The feed consisted of 25 mg/L bacto peptone, 25 mg/L yeast extract, 95 mg/L NH_4Cl, 80 mg/L $NaHCO_3$, 30 mg/L K_2CO_3, 25 mg/L K_2HPO_4, 10 mg/L KH_2PO_4, 11.25 mg/L $MgSO_4{\cdot}7H_2O$, 13.75 mg/L $CaCl_2{\cdot}2H_2O$, 0.125 mg/L $FeCl_3{\cdot}6H_2O$, 0.0112 $MnSO_4{\cdot}H_2O$ mg/L, 0.0007 mg/L $CuSO_4$, 0.0004 mg/L $Na_2MoO_4{\cdot}2H_2O$, and 0.012 mg/L $ZnSO_4{\cdot}7H_2O$. The pH of the feed was 7.2–7.6. A recirculation pump was used to completely mix the reactor bulk solution with a recycling ratio of 15. The reactor bulk solution was aerated to maintain a dissolved oxygen (DO) level of 2–4 mg/L.

Biofilms were taken from the reactor after achieving a quasi-steady state indicated by a constant COD removal efficiency above 90%. Five grams of biofilm were taken each time from the reactor and diluted in 10 mL phosphate buffered saline (PBS). The PBS was prepared by dissolving 1.093 g/L NaH_2PO_4, 0.3175 g/L $NaHPO_4{\cdot}H_2O$, and 8.475 g/L NaCl in ultrapure water (Millipore Corp., MA). Two different bacteria samples were used in the experiment; biofilm bacteria with EPS and biofilm bacteria without soluble EPS. Bacteria with EPS were prepared by vortexing (Fisher Scientific, IL) the biofilm suspension at the maximum speed for 1 min. In order to strip off the soluble EPS, the biofilm suspension was vortexed for 1 min at the maximum speed, followed by centrifuging the cell suspension at 3500 rpm for 10 min. After decanting the supernatants, the pellets were resuspended in PBS. The centrifugation and pellet resuspension steps were repeated once. Bacterial cell suspensions were kept at 4 °C prior to the photocatalytic experiments. The size and shape of the biofilm bacteria with and without EPS were observed by scanning electron microscopy (SEM).

2.3. E. coli cell preparation

The stored *E. coli* (strain JM109) were streaked onto Luria–Bertani (LB) agar plates and incubated at 37 °C overnight. *E. coli* cells were cultivated in a shaking incubator (New Brunswick Scientific Co., NJ) in LB broth at 200 rpm and 37 °C for 20 h. The culture was harvested by centrifugation (Beckman Coulter, CA) at 3000 × *g* and 4 °C for 10 min and washed three times with PBS buffer. Cell suspensions with an *E. coli* concentration of approximately 10^8 colony forming units (CFU)/mL were obtained by observing their optical density (OD) at 600 nm using a UV/vis spectrophotometer (Varian, Inc., CA). Cell sus-

pensions were kept on ice prior to the experiments to minimize potential bacterial growth. The cell suspension pH ranged from 7.0 to 7.2.

2.4. Photocatalytic reactions

The photodegradation of bacteria was carried out during the summer in Milwaukee, WI, USA. The solar irradiation intensity was measured with a broad range light meter (Sper Scientific Ltd., AZ). Aqueous suspensions containing photocatalysts were stirred by a magnetic stirrer for 24 h to uniformly disperse nanoparticles prior to each experiment. The stirred nanoparticle suspensions were added to bacterial suspensions and completely mixed by vigorous vortexing. Fifty milliliters of suspensions containing photocatalysts and microorganisms were then transferred to 10 cm diameter petri dishes and exposed to solar light. The concentration of photocatalysts used was 0.1 mg/mL in the aqueous suspension. The average solar intensity was measured at 10 W/m^2 for all experiments. Samples were withdrawn periodically during the course of the reaction and transferred onto ice for further chemical and microbiological analysis.

2.5. Bacterial characterization

2.5.1. Counting techniques

The numbers of viable bacteria were counted within 2 h after samples were withdrawn from the experiments. A series of 10-fold dilutions were performed and 10 μL of each dilution was plated on R2A agar plates in triplicate for the biofilm heterotrophic plate count (HPC) and on LB agar plates for *E. coli* bacteria count. R2A plates were incubated at 37 °C for 20 h and placed at room temperature for two days before the counting was performed. *E. coli* bacteria were counted immediately after the 20 h incubation at 37 °C.

2.5.2. Carbohydrate and protein analysis

To determine changes in the bacterial total carbohydrate concentration and total protein concentration during the course of the photocatalysis, 1 mL cell suspension was withdrawn and placed in a 1.5 mL plastic centrifuge tube, followed by 5 min sonication at 5.0 Hz with a cell disruptor (Branson Sonic Power Co., CN). The bacterial pellets were removed by ultracentrifugation (Beckman Coulter, CA) at 33,000 × *g* and 4 °C for 10 min. Carbohydrates were quantified using the phenol-sulfuric acid method as described by Dubois et al. [30] with glucose as the standard. Proteins were assayed colorimetrically with a bicinchoninic acid (BCA) protein assay kit (Bio-Rad Laboratories, CA). Protein standards were prepared with bovine serum albumin (BSA). The normalized carbohydrate and protein concentrations were obtained by dividing the total carbohydrate and total protein by the biofilm dry weight. The biofilm wet weight was measured immediately after samples were taken from the reactor; the dry weight was obtained after drying the original biofilm in an oven at 105 °C until a constant weight was achieved.

3. Results and discussion

3.1. Synthesis and characterization of new photocatalysts—visible light sensitivity

The nitrogen-doped nanoparticles were first analyzed by X-ray photoelectron spectroscopy. Fig. 1 shows the full-scale XPS spectra of the doped TiO_2 and ZrO_2. All spectra were calibrated with respect to the C 1s peak at 284.6 eV. In the XPS spectra, all the features of metal oxides and an additional N 1s with binding energy of 399.4 eV for N-doped TiO_2 and ZrO_2 (ethylenediamine based), 398.6 eV for N-doped TiO_2 (ethanolamine based) can be seen clearly. The nitrogen levels obtained from XPS spectra are 17% for N-doped TiO_2 prepared from ethylenediame, 16% for N-doped TiO_2 prepared from ethanolamine and 7% for N-doped ZrO_2 from ethylenediamine.

Fig. 2 shows the UV–vis reflectance spectra of N-doped TiO_2 and ZrO_2 nanoparticles and a reference spectrum of pure TiO_2 nanoparticles. N-doped TiO_2 nanoparticles exhibit visible light absorption up to 800 nm, while $ZrO_{2-x}N_x$ nanoparticles show an absorption onset around 750 nm. These results indicate that the absorption of the N-doped materials extends well into the visible light region, which may facilitate their induced photocatalytic activity.

3.2. SEM images of biofilm bacteria

Bound EPS contains sheaths, capsular polymers, condensed gel, loosely bound polymers, and attached organic material, while soluble EPS is composed of soluble macromolecules, colloids and slimes. Fig. 3 shows SEM images of biofilm bacteria with intact EPS and biofilm bacteria with their soluble EPS stripped off by centrifugation. Extracellular slimes can be clearly seen on the surface of bacterial cells with EPS in Fig. 3A. In contrast, bacterial surfaces are much smoother (Fig. 3B) after the removal of soluble polymeric substances.

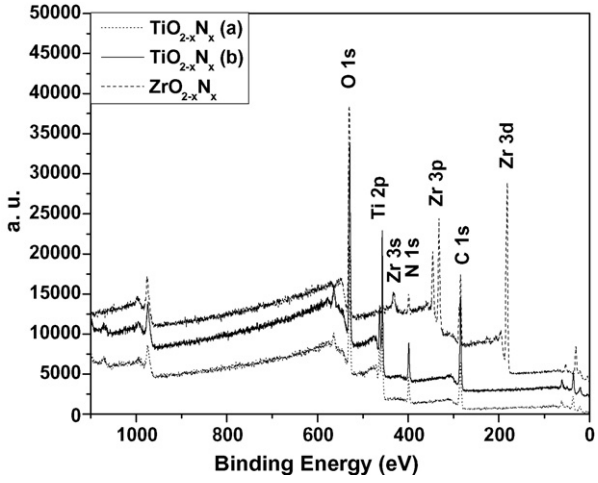

Fig. 1. Full-scale XPS of N-doped metal oxide nanoparticles: $TiO_{2-x}N_x$ ethylenediamine as N source (N% = 17%) (dot), $TiO_{2-x}N_x$ ethanolamine as N source (N% = 16%) (solid), and $ZrO_{2-x}N_x$ ethylenediamine as N source (N% = 7%) (dash).

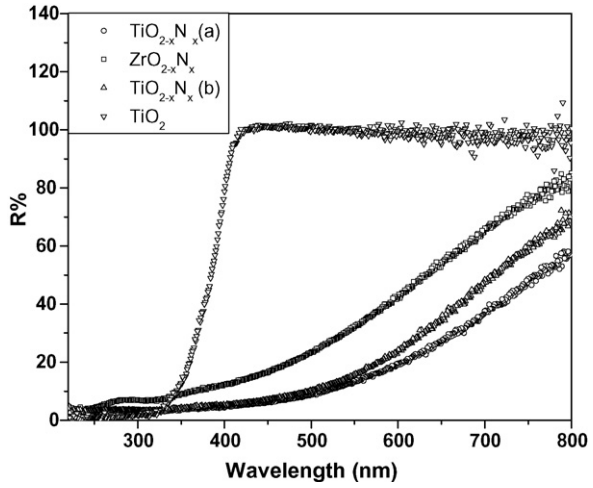

Fig. 2. UV–vis reflectance spectra of N-doped metal oxides and reference TiO_2: $TiO_{2-x}N_x$ ethanolamine as N source, $TiO_{2-x}N_x$ ethylenediamine as N source, $ZrO_{2-x}N_x$ ethylenediamine as N source, and pure TiO_2 nanoparticles.

3.3. Photocatalytic inactivation of bacteria without EPS

The bactericidal performance of N-doped TiO_2 and ZrO_2 nanoparticles was tested on *E. coli* and biofilm bacteria with their EPS stripped off. The bactericidal effects were compared with those obtained with pure TiO_2 nanoparticles. Interactions between bacteria and catalysts in the dark were tested by incubating the bacteria and semiconductor mixed dilutions at room temperature for 24 h. The results revealed no detectable bacterial killing over all photocatalysts by comparing the remaining culturable bacteria number with the culturable bacteria count obtained from dilutions without nanoparticles (data not shown). This indicates that the toxicity of the applied photocatalysts to bacteria is not appreciable under the experimental condition of this study. Photokilling of bacterial cells in the absence of nanoparticles under solar illumination was performed as the control.

Fig. 4A presents the number of culturable biofilm heterotrophic bacteria without soluble EPS remaining in the cell suspension against the solar irradiation time. Results from the experiments without catalysts showed a 3.9 log decrease in HPC after 120 min of solar light illumination with an initial bacteria concentration of 8.9×10^8 CFU/mL. Photocatalysis with all nanoparticles showed improved bactericidal efficiency compared with using the solar light irradiation alone. The HPC removal was 6.3 log after 2 h reaction when pure TiO_2 was used as the photocatalyst. While both $TiO_{2-x}N_x$ and $ZrO_{2-x}N_x$ with ethylenediamine as the N source were significantly more effective than pure TiO_2, the $TiO_{2-x}N_x$ doped with ethylenediamine had the best performance with all heterotrophic bacteria inactivated within 90 min. Moderate improvement in terms of photocatalytic activity was observed when ethanolamine was used as the nitrogen source for $TiO_{2-x}N_x$ compared with pure TiO_2.

Overall, the sequence for the HPC removal efficiency is ethylenediamine-$TiO_{2-x}N_x$ > ethylenediamine-$ZrO_{2-x}N_x$ > ethanolamine-$TiO_{2-x}N_x$ > pure TiO_2 > solar irradiation without catalysts. Although absorption band edge red shift is used consistently as evidence for band gap narrowing, the exact influence of N doping on the band structure is still unclear because the localized N states and Ti^{3+} defect states can also induce similar absorption shifts [31]. The better performance of ethylenediamine-doped materials may be explained by the direct formation of Ti–N bonds. Since in the case of ethanolamine, some of the hydroxyl groups compete with amine groups in the formation of N-bonds to the central Ti ion, the number of directly formed Ti–N bonds is possibly lower in the ethanolamine case compared with the ethlyenediamine case. The Ti–N bond is believed to mediate the electronic coupling between host lattice and dopant, thereby possibly changing the electronic structure at the valence band edge and narrowing the band gap of the metal oxides [7,32]. XPS spectra show that the N 1s peak maximum of $TiO_{2-x}N_x$ (from ethylenediamine) lies at 399.4 eV, while that of the $TiO_{2-x}N_x$ (from ethanolamine) lies at 398.6 eV. The higher binding energy found in the ethylenediamine-$TiO_{2-x}N_x$ compared with the ethanolamine-TiO_2 supports the model that in the previous case N binds to Ti more efficiently than in the later case. ZrO_2 is not well known as a photocatalyst because of its wide band gap and low chemical activity. In our experi-

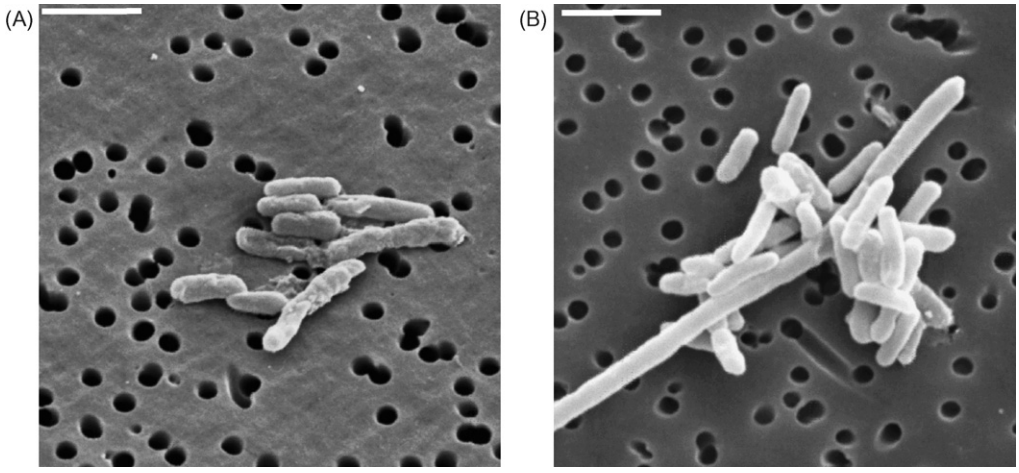

Fig. 3. Scanning electron micrographs of biofilm bacteria with EPS (A), and biofilm bacteria without soluble EPS (B). Bar = 2 μm.

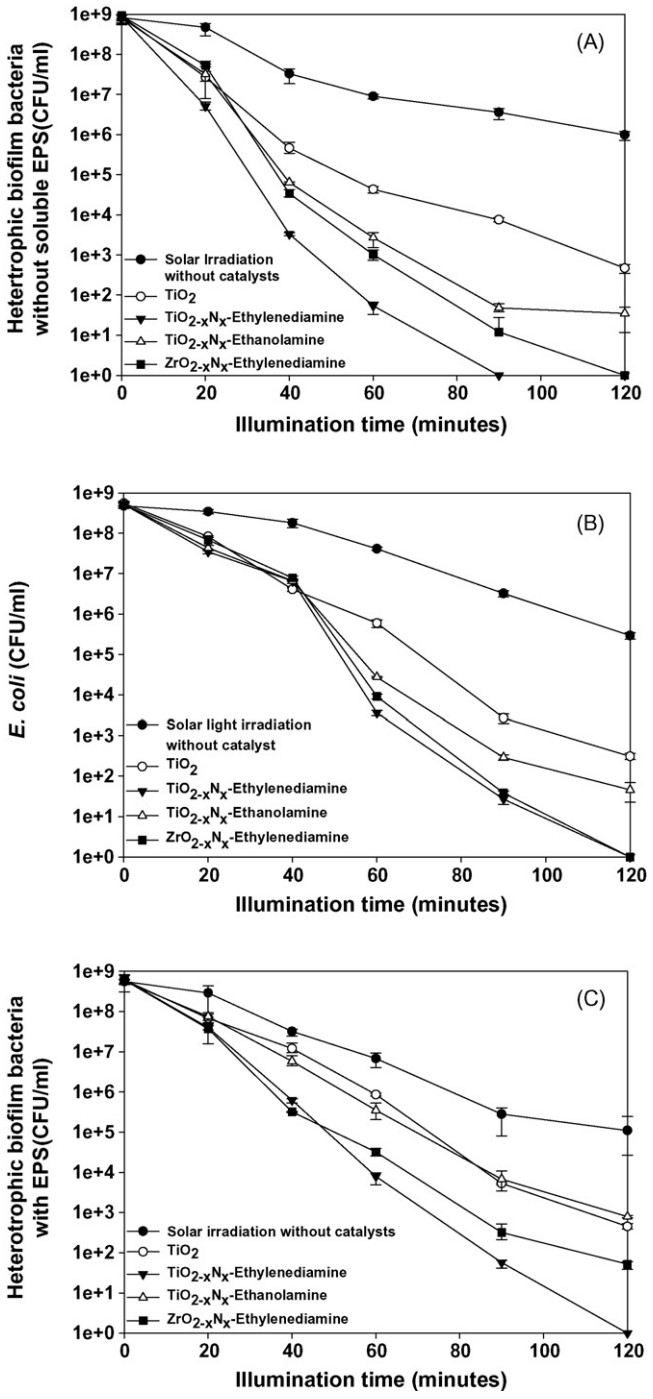

Fig. 4. Inactivation of biofilm heterotrophic bacteria with soluble EPS stripped off (A), *E. coli* JM109 (B), and biofilm heterotrophic bacteria with EPS (C) as a function of solar illumination time. Experimental conditions: initial photocatalyst concentration = 100 mg/L, pH 7.2–7.4, average solar light intensity = 10 mW/cm^2. Error bars represent standard deviations of triplicate measurements.

ments, however, nitrogen-doped ZrO_2 nanoparticles exhibited even better photocatalytic performance compared with pure TiO_2 nanoparticles. It is noticeable that the ethanolamine based $TiO_{2-x}N_x$ nanoparticles shows better visible light sensitivity, but their photocatalytic activity appears to be lower than ethylenediamine sourced $TiO_{2-x}N_x$ and $ZrO_{2-x}N_x$ nanoparticles. The mechanism of the bactericidal activity in $ZrO_{2-x}N_x$ nanoparticles seems to be analogous to $TiO_{2-x}N_x$. More importantly, it is very likely the doping method used in our study can be applied to other metal oxides for modifying the chemical and physical properties, thereby greatly extending their range of applications.

The photocatalytic inactivation of heterotrophic bacteria with their soluble EPS stripped off can be divided into three phases: (1) during the first 20 min, a relatively slower initial photodegradation rate was observed, which could be attributed to the bacterial defense to the ROS attack on the cell membrane [9]; (2) from 20 to 40 min, ROS generation overcame the bacterial defense system; as a result, the HPC decreased rapidly; (3) the inactivation of bacteria became slower for the rest of the experimental period, possibly caused by the competition for ROS between the remaining active bacterial cells and the cell material released during the photocatalytic process.

The photo-degradation of *E. coli* bacteria is shown in Fig. 4B. All four types of catalysts experienced a longer first stage (40 min) of slow bacterial cell removal with similar rates, indicating that catalyst activity was not the rate limiting step during the initial membrane destruction step. After 40 min of illumination, *E. coli* was destructed at faster rates with ethylenediamine-$TiO_{2-x}N_x$ > ethylenediamine-$ZrO_{2-x}N_x$ > ethylenediamine-$TiO_{2-x}N_x$ > pure TiO_2 nanoparticles, which is consistent with the results obtained from biofilm bacteria without EPS in terms of the photocatalysts bactericidal efficiency. A third stage with a slower bactericidal rate was observed from 60 to 120 min for the *E. coli* bacteria inactivation. *E. coli* bacteria and the majority of the biofilm bacteria are gram-negative cells, with outer membranes (lipid bilayer) containing primarily lipopolysaccharides (LPS) and protein. β-proteobacteria and γ-proteobacteria represent a major fraction of the microbial community found in the activated sludge of municipal sewage-treatment plants, where the biofilm reactor seed was obtained from. *E. coli* cells belong to the γ-proteobacteria. Biofilm contains a diverse range of cell types with different features in their LPS, outer membrane proteins, fimbriae, flagella, and EPS, which may explain the greater self defense capability of the *E. coli* bacteria compare with the average mixed culture biofilm bacteria.

3.4. Impact of EPS on the bacteria inactivation mechanism

Fig. 4C shows the solar inactivation of biofilm heterotrophic bacteria with EPS. Significantly lower cell abatement rates were observed for all three types of N-doped nanoparticles compared with their counterparts with soluble EPS stripped off under identical experimental conditions. The inactivation pattern of biofilm bacteria with EPS showed no major distinction between different phases. The slower degradation rates for biofilm bacteria with EPS may be caused by the competition between EPS and bacterial cells for ROS. Both types of biofilm bacteria showed similar removal rates with solar irradiation alone and pure TiO_2. This implies that the presence of EPS played a less important role in controlling the bactericidal kinetics when ROS concentration was reduced.

3.5. Analysis of carbohydrate and protein concentrations

Polysaccharides (carbohydrate polymers) are the main component of biofilm EPS. Inside bacterial cells, polysaccharides are present primarily in the cell wall, while proteins are found throughout the cell, both as parts of cell structures and as enzymes [26]. We analyzed both the total protein and total carbohydrate associated with the bacterial cells during the course of the photocatalytic reactions. The different degradation kinetics for carbohydrate and protein provide valuable information as to whether EPS plays a role in controlling the bacterial decomposition kinetics. Fig. 5 depicts the carbohydrate concentration change for the biofilm bacteria without soluble EPS (Fig. 5A) and the biofilm bacteria with EPS (Fig. 5B) during their photodegradation. By comparing the initial conditions presented in Fig. 5A and B, approximately 28% of the total carbohydrate was associated with the biofilm soluble EPS. Solar light alone did not significantly alter the bacterial carbohydrate content, even though the cells already had lost their viability. Overall, the carbohydrate decomposition kinetics followed a first order exponential decay. The first order carbohydrate removal rate coefficient, k, can be calculated from the following equation:

$$k = \frac{1}{t} \ln \frac{C}{C_0} \quad (1)$$

with t being the reaction duration, C the reactant concentration at time t, and C_0 is the initial reactant concentration. As shown in Fig. 5, total carbohydrate degradation occurred immediately after the irradiation started when the photocatalysts were present. The first order carbohydrate removal rates for biofilm bacteria with EPS was $k = 0.0078\ \text{min}^{-1}$ when pure TiO_2 was used as the photocatalyst, and $k = 0.0092\ \text{min}^{-1}$ when $TiO_{2-x}N_x$-ethylenediamine was used. Significantly higher carbohydrate degradation rates ($k = 0.0101\ \text{min}^{-1}$ for pure TiO_2 and $k = 0.0159\ \text{min}^{-1}$ for $TiO_{2-x}N_x$-ethylenediamine) were achieved for bacteria without soluble EPS.

Fig. 6A and B show the time course of protein degradations for both types of biofilm bacteria. It is noted that the initial protein concentrations are essentially the same regardless of the presence of soluble EPS, indicating that proteins are mainly enclosed within the cell structure. The kinetics of protein degradation follows a pattern similar to carbohydrate degradation with slower initial reactions rates during the first 40 min,

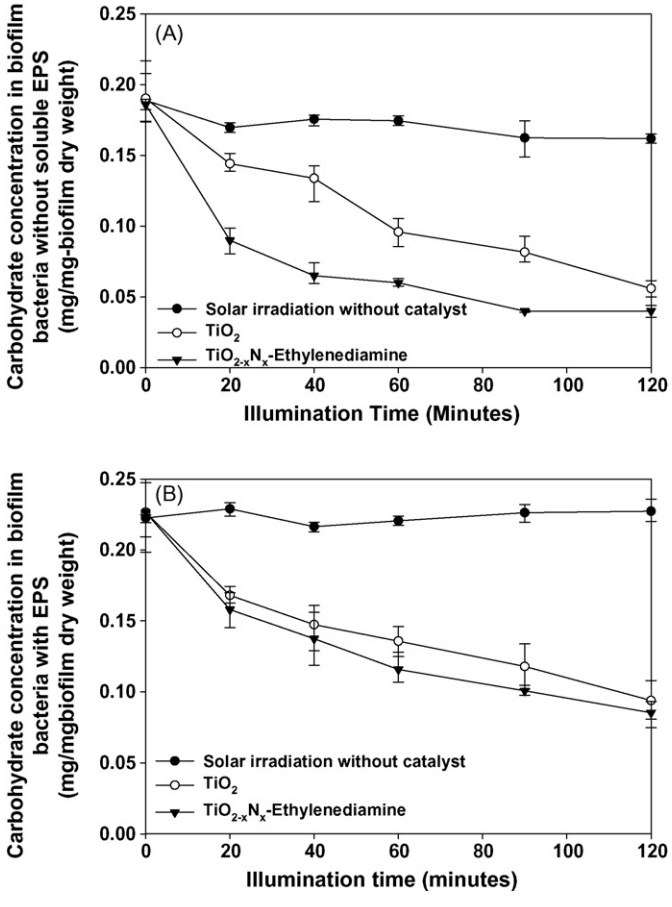

Fig. 5. Carbohydrate degradation of biofilm bacteria with soluble EPS stripped off (A) and the biofilm bacteria with EPS (B) during the photocatalysis. Symbols represent the normalized bacterial carbohydrate (total carbohydrate/bacterial dry weight). Experimental conditions: initial photocatalyst concentration = 100 mg/L, pH 7.2–7.4, average solar light intensity = 10 mW/cm^2. Error bars represent standard deviations of triplicate measurements.

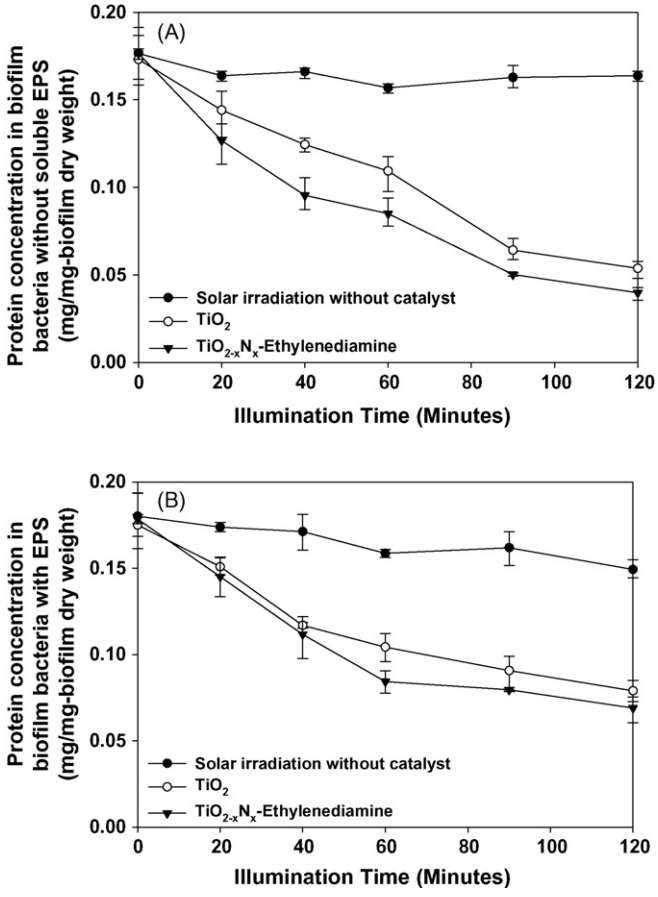

Fig. 6. Protein degradation of biofilm bacteria with soluble EPS stripped off (A) and the biofilm bacteria with EPS (B) during the photocatalysis. Symbols represent the normalized bacterial protein (total protein/bacterial dry weight). Experimental conditions: initial photocatalyst concentration = 100 mg/L, pH 7.2–7.4, average solar light intensity = 10 mW/cm^2. Error bars represent standard deviations of triplicate measurements.

which could be explained by the fact that exopolysaccharides are present at the outermost layer of the bacterial cells. The first order protein degradation rate coefficients were 0.0073 and 0.0098 min^{-1} for biofilm bacteria with EPS and without EPS, respectively, when pure TiO_2 was used, and 0.0091 and 0.0131 min^{-1} for biofilm bacteria with and without EPS when $TiO_{2-x}N_x$-ethylenediamine was used. It should be noted that the removal of protein and carbohydrate for the biofilm bacteria without soluble EPS was faster than that of the biofilm bacteria with EPS for almost all photocatalysts, which is in agreement with the bacterial cell inactivation results.

4. Conclusions

In this study, we successfully used visible light sensitive N-doped TiO_2 and ZrO_2 nanoparticles to achieve significant improvements in biofilm and *E. coli* bacteria photodegradation efficiency. We also found that different nitrogen sources yield $TiO_{2-x}N_x$ with different photocatalytic performance, which could be explained by the different binding sites of N dopants in a given metal oxide matrix.

The abatement of *E. coli* and biofilm bacteria without EPS showed distinctive kinetic patterns indicating the complexity of bactericidal degradation. Removing the soluble EPS from heterotrophic biofilm bacteria significantly increased the bactericidal efficiency for most of the photocatalysts. EPS is found to play an important role in controlling the bactericidal reaction kinetics through competition for ROS with biofilm bacteria. The degradation of cellular substances takes a much longer time to achieve compared with cell inactivation, although the oxidation of carbohydrate and protein followed similar trend as the bacterial killing. The results of our observations suggest that not all types of organism can represent the mixture of bacteria in a natural environment, e.g., biofilm. These findings suggest that nitrogen-doped TiO_2 has potential applications in the development of alternative disinfectants for environmental and medical usage.

References

[1] A. Hagfeldt, M. Gratzel, Chem. Rev. 95 (1995) 49–68.
[2] A.L. Linsebigler, G. Lu, J.T. Yates, Chem. Rev. 95 (1995) 735–758.
[3] C. Burda, X. Chen, R. Narayanan, M.A. El-Sayed, Chem. Rev. 105 (2005) 1025–1102.
[4] A. Mills, S.L. Hunte, J. Photochem. Photobiol. A: Chem. 108 (1997) 1–35.
[5] A. Fujishima, K. Honda, Nature 238 (1972) 37–38.
[6] J.C. Yu, W. Ho, J. Yu, H. Yip, P.K. Wong, J. Zhao, Environ. Sci. Technol. 39 (2005) 1175–1179.
[7] R. Asahi, T. Morikawa, T. Ohwaki, K. Aoki, Y. Taga, Science 293 (2001) 269–271.
[8] C. Burda, Y. Lou, X. Chen, A.C.S. Samia, J. Stout, J.L. Gole, Nano Lett. 3 (2003) 1049–1051.
[9] S.U.M. Khan, M. Al-Shahry, W.B. Ingler Jr., Science 297 (2002) 2243–2245.
[10] C.H. Park, S.B. Zhang, S.H. Wei, Phys. Rev. B 66 (2002) 073202.
[11] S. Sakthivel, H. Kisch, Chem. Phys. Chem. 4 (2003) 487–490.
[12] J.L. Gole, J.D. Stout, C. Burda, Y. Lou, X. Chen, J. Phys. Chem. B 108 (2004) 1230–1240.
[13] S.M. Prokes, J.L. Gole, X. Chen, C. Burda, W.E. Carlos, Adv. Funct. Mater. 15 (2005) 161–167.
[14] R. Bacsa, J. Kiwi, T. Ohno, P. Albers, V. Nadtochenko, J. Phys. Chem. B 109 (2005) 5994–6003.
[15] X. Chen, Y. Lou, A.C.S. Samia, C. Burda, J.L. Gole, Adv. Funct. Mater. 15 (2005) 41–49.
[16] X.F. Qiu, Y.X. Zhao, C. Burda, Adv. Mater., submitted for publication.
[17] Y. Liu, X. Chen, J. Li, C. Burda, Chemosphere 61 (2005) 11–18.
[18] Y. Liu, J. Li, X. Qiu, C. Burda, Wat. Sci. Technol. 54 (8) (2006) 47–54.
[19] K. Sunada, T. Watanabe, K. Hashimoto, J. Photochem. Photobiol. A: Chem. 156 (2003) 227–233.
[20] R.J. Watts, S. Kong, M.P. Orr, G.C. Miller, B.E. Henry, Wat. Res. 29 (1995) 95–100.
[21] M. Cho, H. Chung, W. Choi, J. Yoon, Appl. Environ. Microbiol. 71 (2005) 270–275.
[22] G. Gogniat, M. Thyssen, M. Denis, C. Pulgarin, S. Dukan, FEMS Microbiol. Lett. 258 (2006) 18–24.
[23] Y. Weng, Y. Wang, J.B. Asbury, H.N. Ghosh, T. Lian, J. Phys. Chem. B 104 (2000) 93–104.
[24] A.G. Rincon, C. Pulgarin, Appl. Catal. B: Environ. 49 (2004) 99–112.
[25] V. Nadtochenko, N. Denisov, O. Sarkisov, D. Gumy, C. Pulgarin, J. Kiwi, J. Photochem. Photobiol. A: Chem. 181 (2006) 401–407.
[26] M.T. Madigan, J.M. Martinko, Brock Biology of Microorganisms, Prentice Hall, New Jersey, 2006.
[27] J. Li, S. McLellan, S. Ogawa, Wat. Res. 40 (2006) 3023–3028.
[28] Y. Liu, C.-H. Yang, J. Li, Environ. Sci. Technol. 41 (2007) 198–205.
[29] J. Li, P.L. Bishop, J. Environ. Eng. Sci. 3 (2004) 523–528.
[30] M. Dubois, K.A. Gilles, J.K. Hamilton, P.A. Rebers, F. Smith, Anal. Chem. 28 (1956) 350–356.
[31] Y. Nakano, T. Morikawa, T. Ohwaki, Y. Taga, Appl. Phys. Lett. 86 (2005) 132104.
[32] Z. Lin, A. Orlov, R.M. Lambert, M.C. Payne, J. Phys. Chem. B 109 (2005) 20948–20952.